Additive-free synthesis of 3D porous V2O5 hierarchical microspheres with enhanced lithium storage properties

Chaofeng Zhang
University of Wollongong, czhang@uow.edu.au

Zhixin Chen
University of Wollongong, zchen@uow.edu.au

Zaiping Guo
University of Wollongong, zguo@uow.edu.au

Xiong Wen Lou
Nanyang Technological University

Additive-free synthesis of 3D porous V2O5 hierarchical microspheres with enhanced lithium storage properties

Abstract

A facile synthesis of novel 3D porous V2O5 hierarchical microspheres has been developed, based on an additive-free solvothermal method and subsequent calcination. Due to their unique structure, these V2O5 microspheres display a very stable capacity retention of 130 mA h g (1) over 100 cycles at a current rate of 0.5 C, and show excellent rate capability with a capacity of 105 mA h g (1) even at the 30 C rate. The good electrochemical performance suggests that this unique hierarchical V2O5 material could be a promising candidate as a cathode material for lithium-ion batteries.

Keywords

additive, free, synthesis, 3d, porous, storage, v2o5, properties, hierarchical, microspheres, enhanced, lithium

Disciplines

Engineering | Science and Technology Studies

Publication Details

ARTICLE TYPE

Additive-free synthesis of 3D porous V_2O_5 hierarchical microspheres with enhanced lithium storage properties

Chaofeng Zhang,[a,b,c] Zhixin Chen,[a] Zaiping Guo*[a,c] and Xiong Wen (David) Lou*[b]

A facile synthesis of novel 3D porous V_2O_5 hierarchical microspheres has been developed, based on an additive-free solvothermal method and subsequent calcination. Due to their unique structure, these V_2O_5 microspheres display a very stable capacity retention of 130 mA h g^{-1} over 100 cycles at a current rate of 0.5 C, and show excellent rate capability with a capacity of 105 mA h g^{-1} even at the 30 C-rate. The good
10 electrochemical performance suggests that this unique hierarchical V_2O_5 material could be a promising candidate as a cathode material for lithium-ion batteries.

1. Introduction

Lithium-ion batteries (LIBs), currently the predominant power source for portable electronics, are continuing to attract great
15 interest as the promising power source for electric vehicles (EVs) and hybrid electric vehicles (HEVs), owing to their high energy density and long lifespan.[1, 2] Their commercial use in EVs, however, is still hindered by their low power density and poor rate performance.[2] To meet the demands for use in EVs and
20 HEVs, substantial efforts have been dedicated to finding new competitive electrode materials and new structures.[1-4]

Among the potential cathode materials, V_2O_5 has been intensively studied in recent years for application in LIBs, due to its high energy density, ease of synthesis, and low cost.[5-10] V_2O_5
25 still suffers, however, from low electric conductivity (10^{-2} to 10^{-3} S cm^{-1}), poor structural stability, and a low Li$^+$ ion diffusion coefficient ($\sim 10^{-12}$ cm^2 s^{-1}), resulting in limited long-term cycling stability.[11] In recent years, various structures reported with different performance suggest that the characteristics of V_2O_5,
30 such as the dimensions, morphology, porosity, and texture, are critically important to the electrochemical performance of the electrodes.[5, 12-17] In particular, V_2O_5 nanostructures (such as nanotubes, nanofibers, nanoparticles, nanowires, nanorods, and mesoporous structures) have been demonstrated effective to
35 improve the electrochemical kinetics, shorten the diffusion distance for Li$^+$ ions, and buffer the volume change during the lithium insertion and extraction processes, as compared with non-nanostructured materials.[5, 10, 12, 16, 18] Nevertheless, dispersed nanoparticles may only give very low volumetric energy density,
40 which makes them unsuitable for LIBs in EVs and other large-scale applications.[15] Additionally, some undesirable side reactions or poor thermal stability can emerge due to the extended contact between the electrolyte and the nanosized materials with large surface area, leading to safety hazards and poor cycling
45 stability.[19, 20] Generally, the method of using microsized spherical particles is one possible approach towards high packing density

and decreasing the polarization of the electrolyte in the active layer.[9, 15, 21-26] By comparing the response of micro and nano LiMn$_{0.85}$Fe$_{0.15}$PO$_4$ based electrodes, Sun et al. have clearly
50 demonstrated that the former, due to its compact configuration, largely surpasses the latter in terms of volumetric energy density and rate capability.[20] The ordered superstructures, which are self-assembled and transformed from nanostructures, not only maintain the nanostructural features, but also avoid some side-
55 effects common to nanostructures such as low volumetric energy density and poor thermal stability.[19, 20] Recently, the electrode materials with these structures have been found to be the most suitable for improving the electrochemical performance of LIBs.[15, 21, 27-30] It is therefore highly desirable to prepare
60 microsized V_2O_5 spherical structures composed of nanostructures for the design of high-performance LIBs with both high volumetric energy density and high gravimetric energy density, as well as good rate capability.

In this work, we report a facile additive-free solvothermal
65 method followed by a calcination process for mass production of V_2O_5 microspheres consisting of porous nanofibers. When evaluated as a cathode material for LIBs, the three-dimensional (3D) porous V_2O_5 microspheres manifest significantly improved electrochemical performance in terms of specific capacity,
70 cycling stability, and rate capability.

2. Results and discussion

The detailed preparation process for the V_2O_5 microspheres (V_2O_5-ms) can be found in the Electronic Supplementary Information (ESI). The precursor of V_2O_5-ms was first prepared
75 by a solvothermal method, and then heated to obtain the porous structure of V_2O_5-ms. V_2O_5 nanoparticles (V_2O_5-np) were also synthesized by a similar procedure but with a longer reaction time. The crystal phase of both V_2O_5 samples is first confirmed by their X-ray diffraction (XRD) patterns, as shown in Fig. 1A
80 with the peaks labeled, which demonstrates that all the reflections of the samples are in good agreement with the standard pattern of
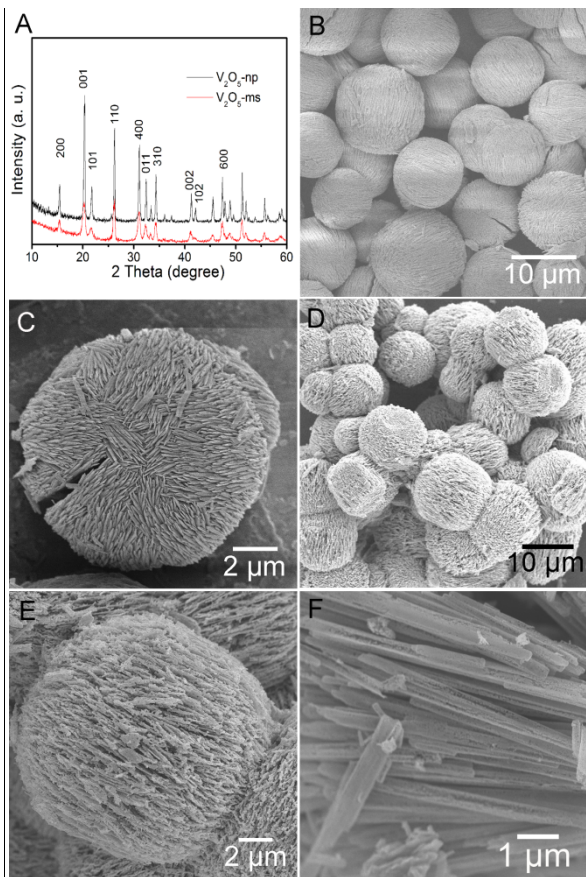
Fig. 1 (A) X-ray diffraction patterns of V$_2$O$_5$-np and V$_2$O$_5$-ms. FESEM images of the precursor of V$_2$O$_5$-ms (B, C), V$_2$O$_5$-ms (D, E), and V$_2$O$_5$-np (F).

Fig. 2 TEM images of V$_2$O$_5$-np (A) and V$_2$O$_5$-ms (B).

35 **Fig. 3** Schematic illustration of the formation of 3D porous V$_2$O$_5$ hierarchical microspheres.

5 pure orthorhombic V$_2$O$_5$ phase (JCPDS card no. 89-0612). No other phases or impurities are detected in the patterns. The morphologies of the two samples are then studied by field-emission scanning electron microscope (FESEM). As shown in Fig. 1B, the as-prepared precursor of V$_2$O$_5$-ms consists of
10 microspheres with good uniformity and a diameter of about 4-10 μm. The high magnification image of a single sphere presented in Fig. 1C shows that the sphere is composed of uniform nanofibers. After the calcination process, the structure of the microspheres is perfectly retained (Fig. 1D), while the nanoporous structure of the
15 nanofibers arises from the decomposition of the precursor. As shown in Fig. 1E, the 3D microspheres are constructed from these nanoporous fibers. This will endow the material with shorter diffusion pathways and easier Li$^+$/electron transport, leading to enhanced electrochemical performance. A FESEM image of
20 V$_2$O$_5$-np obtained with an extended solvothermal reaction time of 24 h is shown in Fig. 1F. It can be observed that the microsphere structure is damaged and porous fibers with a length of several micrometers are loosely distributed over a large domain. In a high-magnification FESEM image, it is easily observed that the
25 V$_2$O$_5$-np fibers consist of nanoparticles with a diameter of 40-100 nm, as indicated in Fig. S1 (see ESI).

The formation of the V$_2$O$_5$-np and V$_2$O$_5$-ms nanostructures is further evidenced by transmission electron microscope (TEM) observations. The primary particle size of V$_2$O$_5$-np (Fig. 2A) is in
30 the range of 40-100 nm, while that of V$_2$O$_5$-ms (Fig. 2B) can be as small as 5-20 nm. In addition, Brunauer-Emmett-Teller (BET)
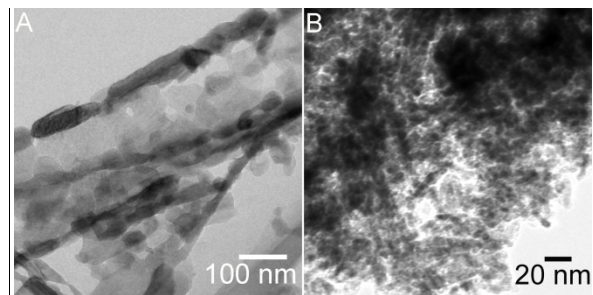
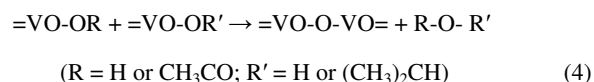measurements show that the specific surface area of V$_2$O$_5$-ms and V$_2$O$_5$-np is 41.6 and 29.2 m^2 g^{-1}, respectively.

It was reported that nanostructured materials can grow into
40 self-assembled microstructures based on an oriented aggregation mechanism.[31-34] Fig. 3 illustrates the proposed growth process for the synthesis of 3D porous V$_2$O$_5$-ms, involving the following four steps: (1) nucleation and growth. In the solvothermal process, the overall reaction of vanadium (V) oxytriisopropoxide (VO(OiPr)$_3$)
45 and acetic acid (HAc) leads to formation of ROVOOR′ (R = H or CH$_3$CO; R′ = (CH$_3$)$_2$CH or H), according to the following reactions: [31]

$$VO(OiPr)_3 + xCH_3COOH \rightarrow (CH_3COO)_xVO(OiPr)_{3-x} + x(CH_3)_2CHOH \qquad (1)$$

50 $$CH_3COOH + (CH_3)_2CHOH \rightarrow CH_3COOCH(CH_3)_2 + H_2O \qquad (2)$$

$$=VO\text{-}OR + H_2O \rightarrow =VO\text{-}OH + ROH$$

$$(R = CH_3CO \text{ or } (CH_3)_2CH) \qquad (3)$$

$$=VO\text{-}OR + =VO\text{-}OR' \rightarrow =VO\text{-}O\text{-}VO= + R\text{-}O\text{-}R'$$

$$(R = H \text{ or } CH_3CO; R' = H \text{ or } (CH_3)_2CH) \qquad (4)$$
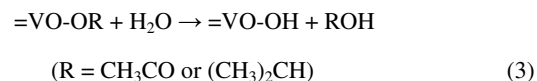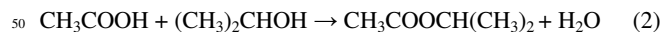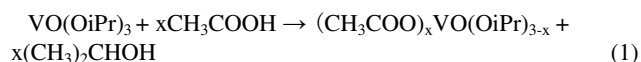
55 VO(OiPr)$_3$ will first react with HAc to produce unstable vanadium acetate complexes (CH$_3$COO)$_x$VO(OiPr)$_{3-x}$ by ligand exchange/substitution (eq. 1). Afterwards, water will be synthesized by the reaction between isopropanol and HAc (eq. 2). Then, due to the hydrolysis-condensation and nonhydrolytic
60 condensation processes, V-O-V bonds would form (eq. 3 and 4). During the reaction, numerous precursor nuclei form quickly and then grow into fiber-like nanocrystals, as shown in the FESEM image of the intermediate product after solvothermal reaction for

5 min (Fig. S2, see ESI). (2) After that, driven by minimization of the overall surface energy, these fiber-like nanocrystals self-aggregate and form microstructured spheres or fan-like structures.[33, 34] As shown in Fig. S3 (see ESI), fan-like bundles of the precursor can be observed after prolonging the reaction time to about 15 min. (3) Oriented aggregation. With longer reaction time, the precursors further aggregate and develop into microsized spheres composed of nanofibers (Fig. S4, see ESI). (4) During the calcination process, the precursors decompose to form the porous V_2O_5 structure.
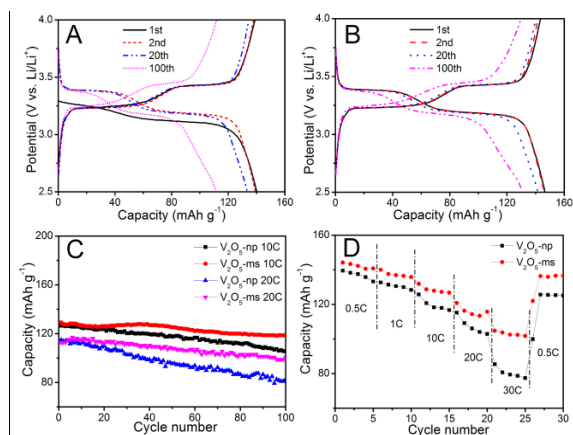

Fig. 4 Charge-discharge voltage profiles of V_2O_5-np (A) and V_2O_5-ms (B) at the current rate of 0.5 C for the selected cycles indicated. (C) Cycling performance of V_2O_5-np and V_2O_5-ms at different current rates (10 C and 20 C). (D) Rate capability of V_2O_5-np and V_2O_5-ms at various current rates.

To demonstrate the possible structural advantages, we have evaluated the electrochemical lithium storage properties of the two samples as cathode materials for LIBs. Fig. 4A shows representative discharge/charge voltage profiles of the V_2O_5-np at a current rate of 0.5 C (75 mA g^{-1}) within a cut-off voltage window of 2.5-4.0 V, which are in good agreement with previous reports.[7, 8, 14] The first discharge of the V_2O_5-np electrode is found to be 140.3 mA h g^{-1}. As shown in Fig. 4B, the V_2O_5-ms electrode shows similar plateaus, but exhibits a larger capacity in the first cycle compared to V_2O_5-np. Specifically, the first discharge capacity is 146.3 mA h g^{-1}, which reaches nearly its theoretical capacity for the transformation from V_2O_5 to LiV_2O_5 (147 mA h g^{-1}).

The cycling performance of the V_2O_5-np and V_2O_5-ms at a current rate of 0.5 C is shown in Fig. S5 (see ESI). The V_2O_5-np sample shows relatively stable capacity retention, although the capacity drops to 111 mA h g^{-1} at the end of the 100th cycle. The V_2O_5-ms sample shows significantly improved cycling performance under the same conditions, as illustrated by its stable capacity retention of 130 mA h g^{-1} after 100 cycles. The cycling performance of the two materials was also investigated at current rates of 10 C and 20 C, as shown in Fig. 4C. When the current rate is increased to 10 C, the capacity retention of V_2O_5-ms upon prolonged cycling is significantly improved over that of V_2O_5-np. A high reversible capacity of 118 mA h g^{-1} is retained after 100 cycles, which corresponds to a capacity loss of only 0.085% per cycle, while the V_2O_5-np electrode suffers a capacity fading rate of 0.165% per cycle. Upon further increasing the current rate to 20 C, a capacity of 113 mA h g^{-1} can still be delivered for V_2O_5-

ms initially, and the capacity is as high as 101 mA h g^{-1} at the end of the 100th cycle. In contrast, the discharge capacity of V_2O_5-np drops dramatically from 114 to 82 mA h g^{-1}. The relevant volumetric capacity at 20 C is presented in Fig. S6 (see ESI). It can be observed that the V_2O_5-ms electrode exhibits significantly higher volumetric capacity with excellent cycling stability compared to the V_2O_5-np electrode. Additionally, the rate capability of V_2O_5-ms is also much better than that of V_2O_5-np, as demonstrated in Fig. 4D. With the benefits of its unique structures, the V_2O_5-ms sample exhibits excellent cycling response to a continuously varying current rate. Even when cycled at the very high rate of 30 C, a high capacity of 105 mA h g^{-1} can still be maintained, as shown in Fig. 4D, while a capacity of only 75 mA h g^{-1} is delivered by the V_2O_5-np sample under the same conditions. After the deep cycling at 30 C, the V_2O_5-ms material can recover nearly the same initial capacity when the current rate is reduced back to 0.5 C. Obviously, the V_2O_5-ms sample exhibits higher capacity at each current rate. The electrochemical performance of the V_2O_5-ms electrodes is good compared to that of many published V_2O_5 electrodes, in terms of high-rate capability and cycling performance (Table S1, see ESI). To investigate the effects of the unique structure on the conductivity, electrochemical impedance spectroscopy (EIS) measurements (Fig. S7, see ESI) were carried out. The charge-transfer resistance R_{ct} for V_2O_5-ms (46 Ω cm^{-2}) is less than 70% of that for V_2O_5-np (73 Ω cm^{-2}), indicating enhanced charge transfer in the V_2O_5-ms electrode. The better performance of V_2O_5-ms is also likely due to the unique structural features. Apparently, the porous nanostructure with high surface area is favourable for alleviating the volume change during charging/discharging processes, as well as for increasing the amount of reactive sites and electrode-electrolyte interface. The hierarchical porous structure thus not only facilitates the kinetics for Li^+ ion diffusion and electron transport by shortening the diffusion pathways to the nanoscale, but also improves the electrode stability because of the reduced lattice strain associated with lithium intercalation.[35, 36] Moreover, the structural robustness of the V_2O_5 microspheres is also perhaps responsible for the improved electrochemical performance.[14, 20]

3. Conclusions

We have successfully prepared 3D porous V_2O_5 hierarchical microspheres on a large scale by an additive-free solvothermal method followed by annealing at 350 °C in air. The as-synthesized V_2O_5 microspheres are composed of well-defined porous nanofibers that arrange themselves in an oriented manner and form a highly porous hierarchical structure. Such porous microspheres give rise to high surface area and high volumetric energy density. Meanwhile, the electronic/ionic transport and the ability to buffer the volume variation are also improved due to the unique porous structure of the microspheres. When evaluated as a cathode material for lithium-ion batteries, the V_2O_5 microspheres display relatively stable capacity retention at different current rates. They also show excellent rate capability, with a capacity of 105 mA h g^{-1} at the 30 C-rate. The excellent electrochemical performance suggests that these unique hierarchical V_2O_5 microspheres could be a promising cathode material for lithium-ion batteries.

Acknowledgments

Notes and references

a *School of Mechanical, Materials & Mechatronics Engineering, University of Wollongong, NSW 2500, Australia. Email: zguo@uow.edu.au*

b *School of Chemical and Biomedical Engineering, Nanyang Technological University, 62 Nanyang Drive, Singapore, 637459. Email: xwlou@ntu.edu.sg*

c *Institute for Superconducting & Electronic Materials, University of Wollongong, NSW 2500, Australia*

† Electronic Supplementary Information (ESI) available: Experimental details and characterizations. See DOI: 10.1039/b000000x/

1. P. G. Bruce, S. A. Freunberger, L. J. Hardwick and J. M. Tarascon, *Nat. Mater.*, 2012, **11**, 19.
2. M. Armand and J. M. Tarascon, *Nature*, 2008, **451**, 652.
3. P. G. Bruce, B. Scrosati and J. M. Tarascon, *Angew. Chem. Int. Ed.*, 2008, **47**, 2930.
4. C. F. Zhang, C. Q. Feng, P. Zhang, Z. P. Guo, Z. X. Chen, S. Li and H. K. Liu, *RSC Adv.*, 2012, **2**, 1643.
5. Y. Wang, K. Takahashi, K. Lee and G. Z. Cao, *Adv. Funct. Mater.*, 2006, **16**, 1133.
6. Y. Wang and G. Z. Cao, *Adv. Mater.*, 2008, **20**, 2251.
7. G. D. Du, K. H. Seng, Z. P. Guo, J. Liu, W. X. Li, D. Z. Jia, C. Cook, Z. W. Liu and H. K. Liu, *RSC Adv.*, 2011, **1**, 690.
8. K. H. Seng, J. Liu, Z. P. Guo, Z. X. Chen, D. Z. Jia and H. K. Liu, *Electrochem. Commun.*, 2011, **13**, 383.
9. A. M. Cao, J. S. Hu, H. P. Liang and L. J. Wan, *Angew. Chem. Int. Ed.*, 2005, **44**, 4391.
10. Y. S. Hu, X. Liu, J. O. Muller, R. Schlogl, J. Maier and D. S. Su, *Angew. Chem. Int. Ed.*, 2009, **48**, 210.
11. L. Q. Mai, L. Xu, C. H. Han, X. Xu, Y. Z. Luo, S. Y. Zhao and Y. L. Zhao, *Nano Lett.*, 2010, **10**, 4750.
12. T. Y. Zhai, H. M. Liu, H. Q. Li, X. S. Fang, M. Y. Liao, L. Li, H. S. Zhou, Y. Koide, Y. Bando and D. Goberg, *Adv. Mater.*, 2010, **22**, 2547.
13. D. M. Yu, C. G. Chen, S. H. Xie, Y. Y. Liu, K. Park, X. Y. Zhou, Q. F. Zhang, J. Y. Li and G. Z. Cao, *Energy Environ. Sci.*, 2011, **4**, 858.
14. S. Q. Wang, S. R. Li, Y. Sun, X. Y. Feng and C. H. Chen, *Energy Environ. Sci.*, 2011, **4**, 2854.
15. S. Q. Wang, Z. D. Lu, D. Wang, C. G. Li, C. H. Chen and Y. D. Yin, *J. Mater. Chem.*, 2011, **21**, 6365.
16. G. C. Li, C. Q. Zhang, H. R. Peng and K. Z. Chen, *Macromol. Rapid Commun.*, 2009, **30**, 1841.
17. S. Beke, *Thin Solid Films*, 2011, **519**, 1761.
18. Y. Wang, H. J. Zhang, W. X. Lim, J. Y. Lin and C. C. Wong, *J. Mater. Chem.*, 2011, **21**, 2362.
19. H. F. Xiang, H. Wang, C. H. Chen, X. W. Ge, S. Guo, J. H. Sun and W. Q. Hu, *J. Power Sources*, 2009, **191**, 575.
20. Y. K. Sun, S. M. Oh, H. K. Park and B. Scrosati, *Adv. Mater.*, 2011, **23**, 5050.
21. C. W. Sun, S. Rajasekhara, J. B. Goodenough and F. Zhou, *J. Am. Chem. Soc.*, 2011, **133**, 2132.
22. D. Zhu, H. Liu, Y. D. Yao and D. C. Li, *Journal of Inorganic Materials*, 2008, **23**, 43.
23. M. M. Ren, Z. Zhou, X. P. Gao, L. Liu and W. X. Peng, *J. Phys. Chem. C*, 2008, **112**, 13043.
24. J. Liu, Y. C. Zhou, J. B. Wang, Y. Pan and D. F. Xue, *Chem. Commun.*, 2011, **47**, 10380.
25. H. M. Xie, R. S. Wang, J. R. Ying, L. Y. Zhang, A. F. Jalbout, H. Y. Yu, G. L. Yang, X. M. Pan and Z. M. Su, *Adv. Mater.*, 2006, **18**, 2609.
26. A. Q. Pan, H. B. Wu, L. Yu, T. Zhu and X. W. Lou, *Acs Appl. Mater. Interfaces*, 2012, **4**, 3874.
27. G. N. Zhu, H. J. Liu, J. H. Zhuang, C. X. Wang, Y. G. Wang and Y. Y. Xia, *Energy Environ. Sci.*, 2011, **4**, 4016.
28. P. Umek, A. Gloter, M. Pregelj, R. Dominko, M. Jagodic, Z. Jaglicic, A. Zimina, M. Brzhezinskaya, A. Potocnik, C. Filipic, A. Levstik and D. Arcon, *J. Phys. Chem. C*, 2009, **113**, 14798.
29. F. Yu, J. J. Zhang, Y. F. Yang and G. Z. Song, *J. Mater. Chem.*, 2009, **19**, 9121.
30. Q. B. Liu, S. J. Liao, H. Y. Song and Z. X. Liang, *J. Power Sources*, 2012, **211**, 52.
31. J. F. Ye, W. Liu, J. G. Cai, S. A. Chen, X. W. Zhao, H. H. Zhou and L. M. Qi, *J. Am. Chem. Soc.*, 2011, **133**, 933.
32. H. Yang, X. L. Wu, M. H. Cao and Y. G. Guo, *J. Phys. Chem. C*, 2009, **113**, 3345.
33. Y. H. Xiao, S. J. Liu, F. Li, A. Q. Zhang, J. H. Zhao, S. M. Fang and D. Z. Jia, *Adv. Funct. Mater.*, 2012, **22**, 4052.
34. P. Nie, L. F. Shen, F. Zhang, L. Chen, H. F. Deng and X. G. Zhang, *Crystengcomm*, 2012, **14**, 4284.
35. T. Tao, A. M. Glushenkov, C. F. Zhang, H. Z. Zhang, D. Zhou, Z. P. Guo, H. K. Liu, Q. Y. Chen, H. P. Hu and Y. Chen, *J. Mater. Chem.*, 2011, **21**, 9350.
36. Z. Y. Wang, D. Y. Luan, S. Madhavi, Y. Hu and X. W. Lou, *Energy Environ. Sci.*, 2012, **5**, 5252.